IOP Publishing Nanotechnology
Nanotechnology 32 (2021) 505608 (11pp) https://doi.org/10.1088/1361-6528/ac24c3

Microwave plasma-based high temperature dehydrogenation of hydrocarbons and alcohols as a single route to highly efficient gas phase synthesis of freestanding graphene

Ondřej Jašek[1], Jozef Toman[1], Miroslav Šnírer[1], Jana Jurmanová[1], Vít Kudrle[1], Jan Michalička[2], Dalibor Všianský[3] and David Pavliňák[1]

[1] Department of Physical Electronics, Faculty of Science, Masaryk University, Kotlarska 2, 611 37 Brno, Czech Republic
[2] Central European Institute of Technology, Brno University of Technology, Purkynova 123, 612 00 Brno, Czech Republic
[3] Department of Geological Sciences, Faculty of Science, Masaryk University, Kotlarska 2, 611 37 Brno, Czech Republic

E-mail: jasek@physics.muni.cz

Received 6 August 2021
Accepted for publication 8 September 2021
Published 6 October 2021

Abstract

Understanding underlying processes behind the simple and easily scalable graphene synthesis methods enables their large-scale deployment in the emerging energy storage and printable device applications. Microwave plasma decomposition of organic precursors forms a high-temperature environment, above 3000 K, where the process of catalyst-free dehydrogenation and consequent formation of C_2 molecules leads to nucleation and growth of high-quality few-layer graphene (FLG). In this work, we show experimental evidence that a high-temperature environment with a gas mixture of H_2 and acetylene, C_2H_2, leads to a transition from amorphous to highly crystalline material proving the suggested dehydrogenation mechanism. The overall conversion efficiency of carbon to FLG reached up to 47%, three times as much as for methane or ethanol, and increased with increasing microwave power (i.e. with the size of the high-temperature zone) and hydrocarbon flow rate. The yield decreased with decreasing C:H ratio while the best quality FLG (low D/G–0.5 and high 2D/G–1.5 Raman band ratio) was achieved for C:H ratio of 1:3. The structures contained less than 1 at% of oxygen. No additional hydrogen was necessary for the synthesis of FLG from higher alcohols having the same stoichiometry, 1-propanol and isopropanol, but the yield was lower, 15%, and dependent on the atom arrangement of the precursor. The prepared FLG nanopowder was analyzed by scanning electron microscopy, Raman, x-ray photoelectron spectroscopy, and thermogravimetry. Microwave plasma was monitored by optical emission spectroscopy.

Supplementary material for this article is available online

Keywords: high temperature, dehydrogenation, graphene, growth mechanism, microwave plasma

(Some figures may appear in colour only in the online journal)

1. Introduction

Nowadays the low-cost and large-scale synthesis of graphene-based nanomaterials gains growing importance as high volume applications of graphene enters the market. High-temperature plasma-based decomposition of organic precursors is a single-step, environmentally friendly way of producing few-layer graphene (FLG) in the form of powder. In comparison to liquid phase exfoliation [1], the synthesized product exhibits high carbon to oxygen content ratio, low structural disorder, and requires no further processing steps. In temperatures above 3000 K, the system is dominated by thermal processes, and the number of resulting stable solid and gas phase products is greatly simplified. At first, a gas reforming of methane was investigated for hydrogen production and resulting carbon black showed the presence of FLG structures [2]. A direct current (DC) plasma torch system with a hollow cathode was used by Kim *et al* [3] for the decomposition of methane and the size of prepared nanosheets was from 100 to 150 nm with an average thickness of 10 nm. Amirov *et al* [4] used a DC plasma torch in Ar/He with methane to produce porous FLG. Zhong *et al* [5] described the use of gliding arc discharge in $Ar/CH_4/H_2$ mixture for the synthesis of FLG nanosheets and showed how the concentration of carbon species influences the formation of carbon clusters and how the presence of C–H bonds reduces dangling bonds on carbon cluster edges. Sun *et al* [1, 6] used pulsed microwave discharge in Ar/CH_4 and showed that the produced FLG had a high C:O ratio and was biocompatible. Magnetically rotating arc was used by Wang *et al* [7] for the decomposition of methane, ethylene, and acetylene at atmospheric pressure in argon. The synthesis process produced FLG nanosheets from methane, but ethylene produced defective structures and the use of acetylene as a precursor resulted in the synthesis of large amounts of amorphous nanoparticles. A high power (28–35 kW) plasma jet operating in helium/propane-butane was used by Shavelkina *et al* [8] to synthesize FLG and their modeling and plasma diagnostics confirmed C_2H_2 and C_2H as a source of C_2 molecules.

Besides methane, both ethanol and dimethyl ether proved to be excellent precursors for a gas-phase synthesis of FLG. This method was first published by Dato *et al* [9], further investigated by Tatarova *et al* [10] and a model of the synthesis process was developed by Tsyganov *et al* [11]. TIAGO torch was used by Melero *et al* [12] for the synthesis of carbon nanotubes and FLG nanosheets by decomposition of ethanol without any catalyst. The prepared nanosheets exhibited very good crystallinity, a high 2D/G Raman band ratio, without an amorphous phase, and a low amount of defects. Fronczak *et al* [13] investigated the growth of various graphene nanostructures including FLG in radiofrequency plasma jet using a wide range of alcohols. They showed that similar to the results of Dato *et al* [14], besides ethanol, other alcohols possessing O/C ratio from 0.1 to 0.5 produced mostly amorphous structures but with higher carbon yield. High O/C ratio was also necessary for the preparation of FLG using gas-phase catalyst-free detonation technique using acetylene/oxygen mixture [15]. Increasing the O/C ratio led to a decrease of defects i.e. decrease of D/G Raman band intensity ratio, but the yield decreased substantially as well.

While the syntheses of FLG from methane, propane-butane, or ethanol were reported, a successful synthesis and demonstration of the dehydrogenation of acetylene remains elusive with only amorphous structures being prepared up to now. In this paper, we investigate the influence of the C:H ratio during the decomposition of organic precursors in the high-temperature plasma zone and show that controlled dehydrogenation reaction can be used for the gas-phase synthesis of high-quality FLG from acetylene as a basic building block with very high efficiency.

2. Experimental

Gas-phase synthesis of freestanding graphene nanosheets was carried out by decomposition of organic precursors in dual-channel microwave plasma torch. The experimental apparatus consisted of a Sairem solid-state microwave (MW) generator, working at a frequency of 2.45 GHz, powering a coaxial plasma applicator. The reactor chamber consists of a 20 cm long fused silica tube with an 8 cm diameter. The gases were supplied to the discharge chamber through the stainless steel nozzle electrode with two gas channels. The central channel (0.8 mm diameter) in the nozzle axis, was used for the introduction of working gas—argon—with flowrate Q_C in 360–500 sccm range and subsequent ignition of plasma. The secondary channel (annulus with outer radius 8.4 mm and inner radius 7.7 mm) was used for introduction of hydrocarbons—acetylene (2–19 sccm), or alcohols—isopropanol (99.8% p.a. Penta), 1-propanol (99.5% p.a. Penta) precursor vapours (10–20 sccm) into the plasma environment. Alcohol vapours were transported into the reactor by argon carrier gas with flowrate $Q_S = 700$ sccm flowing through a temperature-stabilized bubbler with a liquid precursor. Initially, the discharge was ignited with the central channel argon flow only, then the precursor was added through the secondary channel, and the discharge was left to stabilize. The deposition time was 10 min and after the deposition, the reactor cooled down under Ar atmosphere, then it was opened and the synthesized nanopowder was collected from the reactor walls. More details about the experimental procedure can be found in our previous publications [16, 17].

Samples were imaged with MIRA3 (Tescan, Czech Republic) scanning electron microscope (SEM) with Schottky field emission electron gun and equipped with a secondary electron (SE) and back-scattered electron detectors as well as Oxford Instruments EDX analyzer (Oxford, England). High-resolution electron microscopy (HR-TEM) was carried out using HR-TEM Titan™ Themis 60–300 (Thermo Fisher Scientific, USA) equipped with X-FEG high brightness Schottky electron gun, Wien filter type monochromator, and C_s-image corrector. The TEM imaging was performed at 60 kV of acceleration voltage and resolution around 1 Å was achieved with an excited monochromator decreasing the energy spread of the electron source and with aligned corrector minimizing aberrations of the objective lens. XPS analysis was performed

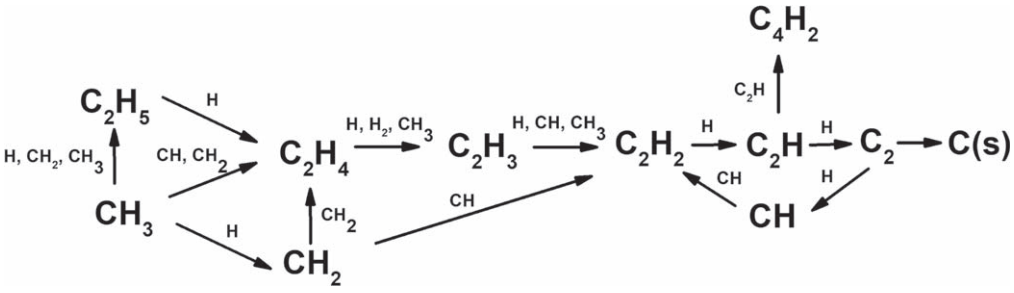

Figure 1. Scheme of reaction mechanism forming acetylene groups and consequently solid carbon according to the model of Tsyganov [11].

using a Thermo Scientific ESCALAB 250Xi x-ray photoelectron spectrometer equipped with a conventional hemispherical analyzer. Monochromatized Al K_α (1486.6 eV) x-ray source was focused into an elliptical spot of 650 μm size. The pass energies were set to 50 eV for wide-scan and 20 eV for high-resolution elemental scans, respectively. These pass energies correspond to energy resolutions of 1.0 and 0.1 eV, respectively. Charge compensation was performed with a self-compensating device using field emitted low energy electrons. Measurements were performed under ultra-high vacuum (10^{-6} Pa) and room temperature. Part of the analysis was also carried out using XPS analysis was performed at a Kratos Analytical Axis Supra (KRATOS-XPS, Kratos Analytical Ltd, UK) spectrometer with a monochromatic Al source using a pass energy of 80 eV for wide spectra and of 20 eV for high-resolution analysis of C 1s, O 1s, N 1s peaks. The analyzed regions were 300 × 700 μm in size. The deconvolution of mentioned peaks was carried out in the CasaXPS 2.3.22PR 1.0 software.

Raman spectroscopy was carried out using the HORIBA LabRAM HR Evolution system with 532 nm laser, using 100× objective, and 5% ND filter (500 mW maximum power), 600 gr mm^{-1} grating, and 60 s acquisition time in the range from 500 to 3350 cm^{-1}.

High-resolution optical emission spectroscopy (OES) was carried out using a Jobin Yvon Triax 550 spectrometer equipped with 1200 and 3600 gr mm^{-1} grating and liquid nitrogen cooled CCD camera. The rotational temperature was estimated by fitting experimentally obtained C_2 ($d^3\Pi_g - a^3\Pi_u$) spectra using the Massive OES software [18, 19].

Thermogravimetric analysis (TGA) with differential thermogravimetry (DTG) was carried out using a Setaram Setsys Evoluton 1750 instrument. The analyses were conducted in a dynamic air atmosphere (20 $sccm^{-1}$) with a constant heating rate of 10 °C min^{-1} in the temperature range from 40 °C to 1000 °C. The obtained data were processed using the Setaram Processing software.

3. Results and discussion

3.1. Synthesis of graphene nanosheets from acetylene

Admixture of hydrocarbons and alcohols, such as methane, acetylene, ethanol, etc to the argon microwave plasma at atmospheric pressure led to a sharp increase of gas temperature, from 1800 to 4500 K, and transition of the reaction mechanism from a low-temperature to a high-temperature regime [20]. In the low-temperature regime, only gaseous products such as hydrocarbons, water, or carbon dioxide are formed. In the high-temperature regime, solid carbon material, hydrogen, carbon monoxide, and simple hydrocarbons are formed. The mechanism for the formation of solid carbon was proposed by Harris *et al* [21] and Frenklach and Wang [22] and it was later suggested that dehydrogenation of main decomposition products such as C_2H_x and CH_y was responsible for the creation of C_2 molecules [9], which form the nuclei and subsequently growth into graphene nanosheet structure. A simplified overview of the reaction mechanism between hydrocarbon groups and atomic hydrogen based on the scheme developed by Marinov [23] and Tsyganov [11] which transforms them into acetylene can be seen in figure 1.

At high enough temperature, acetylene molecules are in the final step dehydrogenated into C_2H and C_2 molecules which, when transported into a colder gas environment below 2000 K, condensate in the graphene nuclei and further grow into the free-standing graphene nanosheets. However, as mentioned above, the direct growth of FLG from acetylene was not observed and only amorphous or highly defective structures were synthesized. Therefore, there must be a significant difference between a pure acetylene environment and other hydrocarbons or alcohols. The pyrolysis of acetylene at temperatures above 1500 K was summarized by Zador *et al* [24] and starts by fission of the C–H bond (enthalpy 413 kJ mol^{-1}) creating an ethynyl radical (C_2H) and an H atom

$$C_2H_2 + M \rightarrow C_2H + H + M, \quad (1)$$

where M is a third-body collider. The produced H atoms can collide with another acetylene molecule forming another ethynyl radical

$$C_2H_2 + H \rightarrow C_2H + H_2. \quad (2)$$

The reaction of ethynyl radicals then forms diacetylene (C_4H_2) and proceeds further to form ($C_{2n}H_2$) molecules

$$C_2H_2 + C_2H \rightarrow C_4H_2 + H. \quad (3)$$

However, this initial reaction has a very low reaction rate (0.02 s^{-1}) and Benson *et al* [25] proposed that reaction of two acetylene molecules forming C_4H_4 is the initial step. C_4H_4 is then converted to vinyl acetylene and forms a more stable C_4H_3 radical by losing the H atom. At high temperatures, the conversion of C_4H_3 and the reaction of two C_2H molecules results in the formation of stable C_4H_2 molecules.

At low temperatures, below 1000 K, the reaction of two acetylene molecules leads to the formation of C_nH_{n+1} molecules which further react with C_2H_2 and prolongate the molecular chain to $C_{n+2}H_{n+3}$ [26]. Benzene, ethylene, and butadiene are important products at low temperatures.

These initial products could become a source for carbon nanomaterial nucleation and growth of FLG. Taking into account the rich chemistry involved in the initial steps of acetylene pyrolysis, the role of acetylene as a principal precursor for solid carbon formation, particularly soot and carbon black, was first suggested by Frenklach and Wang [22]. They proposed the so-called hydrogen abstraction acetylene addition (HACA) mechanism, where a benzene molecule, formed by conversion from acetylene, further grows into more complex aromatic molecules, such as naphthalene, by the addition of another acetylene molecule. As proposed in the HACA mechanism, the addition of acetylene is followed by consecutive hydrogen abstraction, which removes the H atoms during the growth phase from the graphene scaffold, leaving the lattice composed of carbon atoms. As the hexagonal plane grows in lateral dimensions, the hydrogen content of the produced material decreases. Leaving the growth environment, such a structure is then stabilized by carbon–hydrogen bonds on the outer rings.

As seen above, the initial reactions (1–3) of acetylene pyrolysis suggest that there is some potential formation of free hydrogen in the reaction environment, thus we analyzed species formed by the decomposition of acetylene in our discharge by OES. Optical emission spectra of microwave plasma torch discharge in $Ar/C_2H_2/H_2$ mixture can be seen in figure 2. We could observe emission spectra of argon (4s-5p 420 nm, 4p-4s above 690 nm), hydrogen H_α and H_β (656.3 and 486.1 nm), and C atomic line at 247.8 nm in the emission spectra just above the nozzle, where acetylene was decomposed into carbon and hydrogen. Besides these atomic lines, main molecular bands of carbon radical C_2 Swan system ($d^3\Pi_g - a^3\Pi_u$) at 420–620 nm was observed as well as a second positive system of CH ($A^2\Delta - X^2\Pi$ 431 nm) and violet system of CN ($B^2\Sigma^+ - X^2\Sigma^+$, 344–460 nm). The formation of CN is a very fast process with a high cross-section and causes a high-intensity CN emission band (388 nm) even in presence of small atmospheric impurities in the discharge chamber.

In the case of pure Ar/C_2H_2 gas mixture, we observed only a very small intensity of H_α line showing only very little hydrogen generated by pyrolysis of C_2H_2 as expected by the above-discussed reaction schemes. On the other hand, we can clearly observe that the emission spectra of $Ar/C_2H_2/H_2$ gas mixture (figure 2, red top half) showed much higher intensities of CH, C, and H species in comparison to pure C_2H_2 plasma, proving the presence of dehydrogenation reaction products in this region. As expected with the increasing amount of C atoms in the discharge, CN emission band intensity (388 nm) increases as well. This led to the comparable intensity of CN and C_2 (516 nm) molecular band intensities. However, as the nitrogen impurity gets depleted with increasing precursor flow rate, a higher amount of carbon is present in the discharge, the ratio of C_2/CN will substantially increase. Further downstream, 10 mm and more

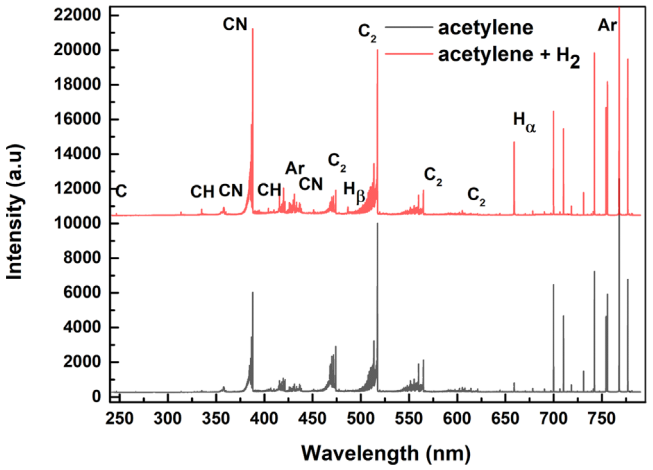

Figure 2. Optical emission spectra of acetylene/H_2 microwave plasma torch discharge just above the plasma nozzle, Q_{C2H2} = 6.5 sccm, Q_{H2} = 0 sccm/13 sccm, P = 195 W.

above the nozzle, we could observe only a strong signal of C_2 and CN molecular bands and the thermal radiation of solid carbon material. The plasma temperature, i.e. neutral gas temperature, in the plasma plume, 15 mm above the nozzle, was determined by fitting of the rotational structure of C_2 band, giving 4500 ± 200 K. Detailed description of the discharge and its plasma diagnostics can be found in our recent publication [27].

At first, we compared the synthesis of carbon nanomaterial under the constant flow rate of acetylene (6.5 sccm), hydrogen either switched on or off, and varying delivered microwave power P = 63–195 W. Under all studied conditions the carbon nanomaterial prepared without the hydrogen admixture resulted in the formation of highly defective carbon nanoparticles (figure 3). The shape and Raman analysis of these nanoparticles are similar to the structure of onion-like shell-shaped carbon nanoparticles observed by Choi *et al* [28] using high-temperature laser irradiation of acetylene. Choi *et al* also suggested that these particles are not formed by the sequence of chemical reactions such as the HACA mechanism, but by direct decomposition of acetylene

$$C_2H_2 \rightarrow C_2 + H_2 \qquad (4)$$

on the surface of growing nanoparticles.

On the other hand, the admixture of hydrogen resulted in the change of nanostructure from highly defective nanoparticles to FLG, if MW power of 100 W and higher was applied (figure 4).

The prepared FLG nanosheets size varied between 150 and 300 nm and slightly increased with an increasing MW power. The few-layer structure consisted of 2–10 layers, 0.5–3 nm thickness, as determined by TEM image analysis (figure 5). The edges of the individual nanosheets were curved and corrugations were observed as well. The curved and closed edges served as a stabilization mechanism to minimize the nanostructure's energy by eliminating high energy dangling bonds [29].

This clear change in the structure of synthesized material was accompanied with the dehydrogenation process of C_2H_2,

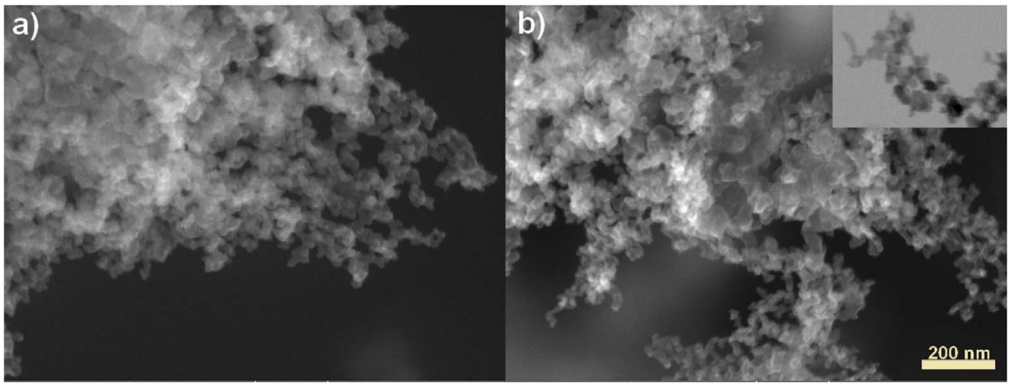

Figure 3. SEM analysis of carbon nanostructures synthesized from C_2H_2 precursor, $Q_{C2H2} = 6.5$ sccm, (a) 130 and (b) 195 W. Inset in (b) STEM image of synthesized nanoparticles.

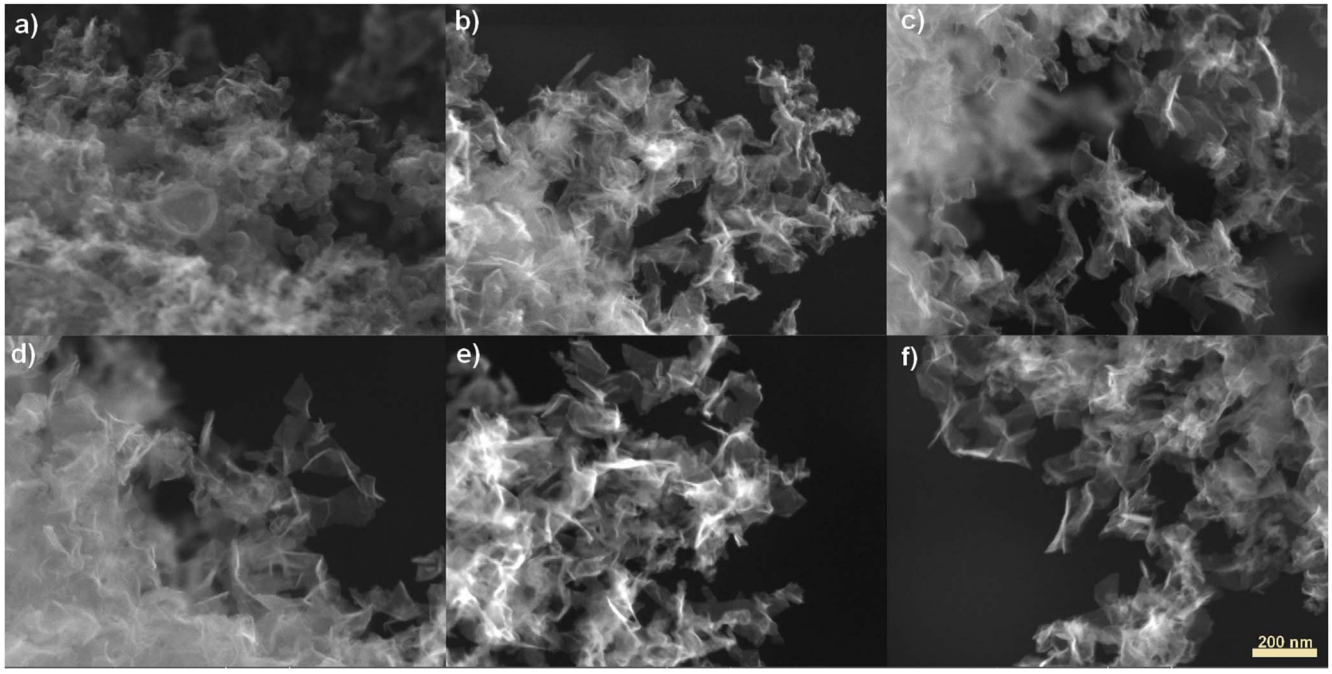

Figure 4. SEM analysis of carbon nanostructures synthesized from C_2H_2/H_2, Q_{C2H2}/Q_{H2} 6.5/13 sccm, precursor: (a) 63 W, (b) 100 W, (c) 130 W, (d) 160 W, and (e) 195 W. Comparison to (f) Q_{C2H2}/Q_{H2} 19/38 sccm with $P = 195$ W.

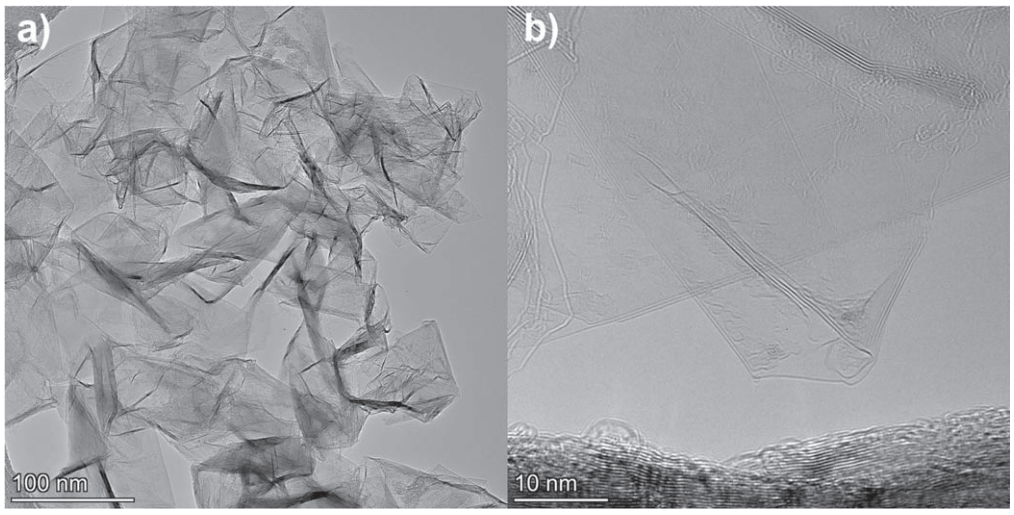

Figure 5. (a) An overview and (b) detailed HR-TEM image of graphene nanosheets synthesized from C_2H_2/H_2 gas mixture.

as shown in figure 2, which generated an increased amount of C and CH species. Increased concentration of C and C_2 species together with increased volume of the high-temperature environment, above 4500 K, led to nucleation and growth of FLG. The importance of the formation of the high-temperature environment for dehydrogenation of the species, such as C_2H by equations (1)–(3), and reaching supersaturation conditions in the carbon gas was recently shown by Shavelkina *et al* [8] in the case of the FLG synthesis from propane-butane. The role of temperature field in the growth of FLG was also discussed in detail by Meunier *et al* [30] showing possible control of thickness and size of the nanosheets by the concentration of CH_4 precursor gas in the high-temperature zone. They argued that the growth was dominated by the incoming carbon condensation flux towards the graphene edge boundaries, but there is also the possibility of inclusion of part of the incoming flux within the existing layers of the graphene structure. The results of their model further suggested that the formation of large amounts of small islands on the top of existing layers would result in the non-uniform nanosheet growth and the loss of structural integrity resulting in the formation of spherical onion-like particles. This is indeed what was observed in the case of pure C_2H_2 precursor synthesis (figure 3) where direct decomposition according to equation (4) could occur. The plasma source stability is also very important for the FLG growth as shown by Toman *et al* [16], as even at a high enough temperature, the spatial and temporal stability of the temperature field leads to the formation of defective structures and an increased amount of higher hydrocarbons and aromatic compounds containing large amounts of hydrogen is produced [21]. Nevertheless, at temperatures of 4000–4500 K, the nucleation and growth of FLG from species such as C_6H_6 and $C_{18}H_{14}$ as suggested by Choi *et al* [31] in the case of CVD graphene growth is not possible because of their low thermal stability.

Therefore, the direct growth from the hydrogen-containing species is rather limited, however, Zhong *et al* [5] recently showed by a molecular dynamic simulation of Ar/CH_4 gas mixture that the enclosure of the graphene hexagonal network was constrained by carbon–hydrogen bonds formed on the nanosheets' edge during its growth preferring the formation of planar graphene structure over enclosed fullerene-like objects. In general, it is very little known about the hydrogen content of gas-phase synthesized graphene. Dato *et al* [32] used mass spectrometry to analyze hydrogen content of the FLG prepared by microwave plasma decomposition of ethanol and only 1 at% or less of hydrogen was detected in the investigated material. This value is not surprising as most of the hydrogen is contained in the volatile hydrocarbon species such as CH_4, C_2H_2, C_2H_4 [33], and H_2 formed during the synthesis and escapes the experimental reactor by exhaust line.

The synthesized material was further analyzed by Raman spectroscopy (figures S1 and S2 (available online at stacks.iop.org/NANO/32/505608/mmedia)). The main Raman bands observed in measured spectra were D (1345 cm^{-1}), G (1580 cm^{-1}), and 2D (2680 cm^{-1}) bands. Low-intensity disorder-related bands, D^*, D^{**}, and D′ at 1210, 1450, and 1610 cm^{-1}, respectively, were also observed in the samples prepared at lower MW power. Second-order modes G^* (2450 cm^{-1}) and D + G (2950 cm^{-1}) could be observed as well. The D/G band integrated intensity ratio value slightly decreased, from 0.6 to 0.5, with increasing MW power and 2D/G band ratio increased as well and reached 1.5 at 195 W (figure 6). The full width at half maximum (FWHM) of 2D peak value was around 50 cm^{-1} in all samples which were consistent with the observed FLG structure [34]. The corrugations and deformations of edges caused an increase of D band intensity in our samples. The highly defective carbon structures exhibited a high-intensity D and G band (figure S1), with D/G ratio of 1.6, and a low-intensity 2D band.

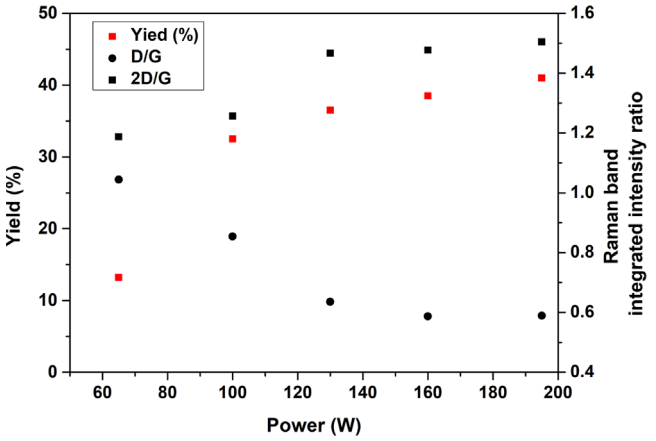

Figure 6. Raman spectra analysis results and yield values for synthesis from a gas mixture of $C_2H_2 + H_2$ with $Q_{C2H2} = 6.5$ sccm, $Q_{H2} = 13$ sccm, $P = 63$–195 W.

Elemental analysis of prepared nanopowders by the fitting of XPS survey spectra in selected element regions (C1s–284 eV, O1s–530 eV) showed high carbon content, between 98.3 and 99.7 at%, the rest being oxygen. Such a high C/O was not observed in alcohol-based gas-phase synthesis of FLG but is consistent with results obtained with methane precursor [6]. No nitrogen content was observed in XPS spectra. C1s peak of XPS spectra (figure S3) showed the presence of peaks centered at 283.8 ± 0.1 eV, 284.4 ± 0.1 eV, and 285.0 ± 0.3 eV, which were assigned to sp, sp^2 and sp^3 hybridized carbon. Low-intensity peaks centered at 286.0 ± 0.2 eV, 286.9 ± 0.2 eV, and 288.1 ± 0.2 eV were assigned to C–O, C=O carbonyl, and O–C=O carboxyl groups, respectively. The carbon–oxygen groups present in our samples are partially due to air impurities in our non-vacuum experimental setup and partially by absorption of oxygen-containing organic compounds from the atmosphere. A shake-up peak at 290.9 ± 2.0 eV was found in the spectra as well. The ratio of sp^2/sp^3 hybridized carbon content was in all samples synthesized from C_2H_2/H_2 gas mixture above 10 and was the highest, 50, for the sample synthesized with a gas mixture of Q_{C2H2}/Q_{H2} (19/38 sccm) at the power of 195 W (figure S3(b)). Highly defective material synthesized from C_2H_2 exhibited sp^2/sp^3 ratio of 5 (figure S3(a)).

TGA and DTG curves of C_2H_2 and $C_2H_2 + H_2$ synthesized nanopowders can be seen in figure 7. There are clear

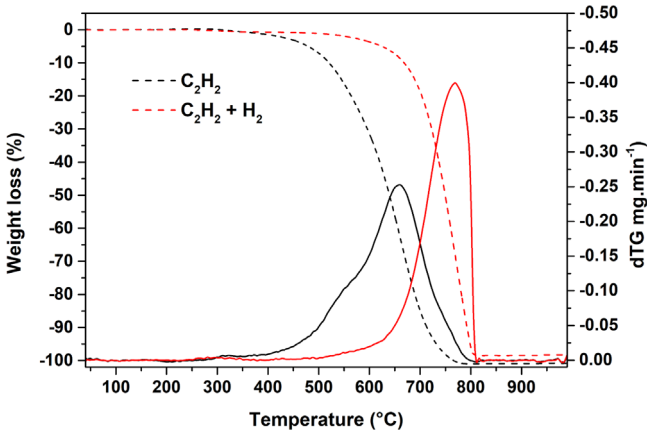

Figure 7. TG (dashed line—left axis) and DTG (solid line—right axis) analysis of FLG prepared from gas mixture of $C_2H_2 + H_2$ with $Q_{C2H2} = 6.5$ sccm, $Q_{H2} = 0/13$ sccm, $P = 195$ W.

differences in thermal stability regions i.e. peak positions of the specific temperature maxima on DTG curves for each type of the studied carbon nanostructures. Defective carbon nanoparticles synthesized from C_2H_2 started to be oxidized above 300 °C and reached maximum decomposition rate at 660 °C. Typical amorphous carbon shows a high decomposition rate between 300 °C and 400 °C, while synthesized nanoparticles decomposition rate was shifted to higher temperatures further suggesting the presence of partially crystalline defective structure. FLG material synthesized from $C_2H_2 + H_2$ mixture remained stable up to 500 °C and peak maximum was observed at 770 °C. No other peaks were observed in the DTG curve profile, thus showing a good quality of the material without an amorphous phase. This result was in agreement with our previous detailed investigation of thermal stability of FLG material synthesized from ethanol precursor using the same experimental setup, that reached DTG curve maximum at 810 °C [35]. This further proved a substantial difference between materials prepared with and without hydrogen admixture.

We further investigated the influence of hydrogen to carbon atomic ratio in synthesis gas mixtures on the FLG properties and nanopowder yield (table 1, figure S4). The nanopowder yield Y_{FLG} [%] was evaluated based on the following equation:

$$Y_{FLG} = (M_{prod}/M_{prec}).100\%, \quad (5)$$

where M_{prod} is mass of obtained carbon nanopowder and M_{prec} is mass of carbon in precursor

$$M_{prec} = t_d.Q_{prec}.Mol_{prec}.C_{prec}, \quad (6)$$

where t_d is synthesis time [minute], Q_{prec} is the precursor flow rate [mol/minute], Mol_{prec} is the molar mass of precursor [g mol^{-1}] and C_{prec} is the relative mass carbon content in precursor i.e. 0.92 for C_2H_2.

The average yield of the synthesis process was slightly increasing with increasing of delivered MW power (figure 6) for the flow rates $Q_{C2H2} = 6.5$ sccm, $Q_{H2} = 13$ sccm and reached 42% at $P = 195$ W. For higher flow rates, up to 19 sccm of C_2H_2 and 38 sccm of H_2, the yield increased to 47%. This is substantially higher than the yield reported in the other works, 10%–14%, [7, 8]. It is also worth noting that although we try to collect all available powder from the reactors' walls and flanges, a very small amount of powder remains on the surfaces and a small part, less than 1%–3% of synthesized material as determined from the weight of the material collected on the fiberglass filters in the exhaust line terminal, could escape the reactor by gas exhaust line, effectively lowering the value of reported synthesis yield.

3.2. Synthesis of graphene nanosheets from higher alcohols

As was mentioned above, ethanol and dimethyl ether were widely used for the synthesis of FLG and it was suggested that their C:H:O ratio is important for the synthesis process. However, synthesis from methane, ethylene and proposed growth mechanism by dehydrogenation of acetylene suggest that oxygen is in fact not needed for the synthesis and one may speculate that it actually lowers the synthesis yield by the formation of a very stable CO molecule, thus removing one carbon from the available amount. To investigate this hypothesis we carried out experiments with two stoichiometrically identical (C_3H_8O) alcohol precursors: 1-propanol ($CH_3CH_2CH_2OH$) and isopropanol ($(CH_3)_2CHOH$). Previously, Fronzcak [13] and Dato [14] reported only highly defective structures being prepared from both precursors.

In comparison to acetylene precursor experiments, we observe two major changes in the optical emission spectra of experiments with 1-propanol and isopropanol. The hydrogen emission lines (H_α, and H_β) intensity increased significantly with the introduction of precursors into the plasma discharge (figure S5) and the intensity of CN molecular band in comparison to C_2 emission band decreased. These changes can be partially attributed to the presence of oxygen in the composition of the precursor and the formation of a more stable CO molecule lowering the amount of carbon available for the formation of CN molecules as well as higher carbon and hydrogen content in the precursor molecule.

To form a stable plasma environment, the experiments were carried out using a constant flow rate of argon ($Q_s = 700$ sccm) through the bubbler with a liquid precursor. The central channel flow rate of argon ($Q_c = 500$ sccm) was constant as well. As a consequence, different vapour pressures of 1-propanol and isopropanol resulted in their different amounts being introduced into the discharge.

SEM and HR-TEM images of the synthesized nanopowders can be seen in figures 8 and 9.

The results showed that 1-propanol ($Q_{1\text{-prop}} = 9$ sccm) as well as isopropanol ($Q_{isoprop} = 19$ sccm), independently of atom arrangement in their respective molecules and without the need for hydrogen admixture, could be used for FLG synthesis. Synthesized nanosheets exhibited very similar characteristics, size of several hundreds of nanometers and morphology, crumpled nanosheets with curved edges, as the samples synthesized using C_2H_2/H_2 mixture.

Raman spectroscopy analysis (figure 10) showed a low D/G band ratio of 0.6 and 2D/G Raman band ratio was 1.6 and 1.4 for 1-propanol and isopropanol, respectively. 2D peak FWHM was slightly broader, 52 cm^{-1}, than in the case of

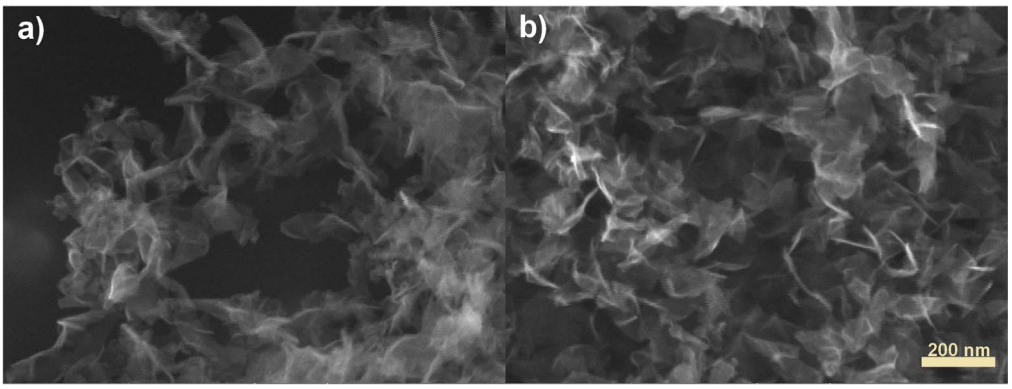

Figure 8. SEM analysis of FLG graphene prepared from isopropanol and 1-propanol precursors, (a) $Q_{\text{isoprop}} = 19$ sccm, (b) $Q_{\text{1-prop}} = 9$ sccm. Argon flow rates $Q_c = 500$ sccm, $Q_s = 700$ sccm and $P = 160$ W.

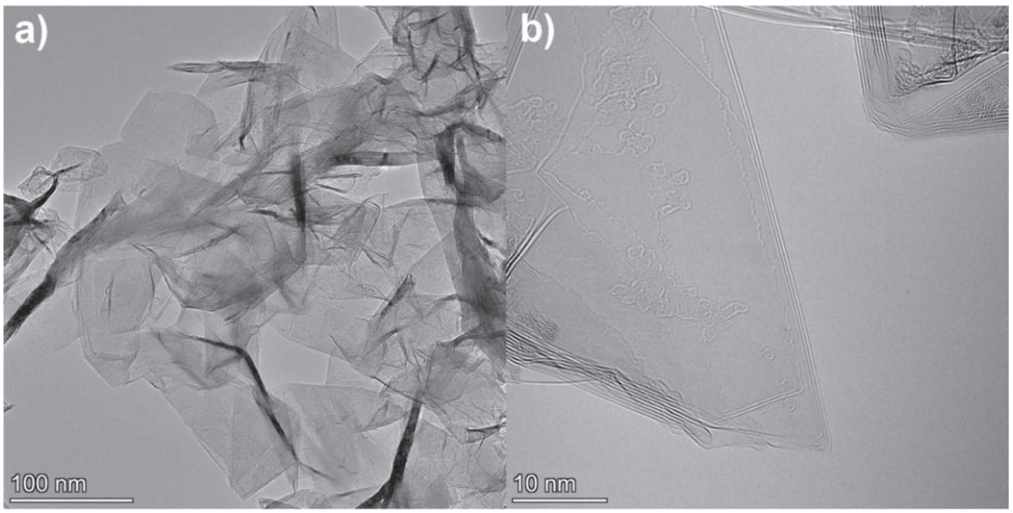

Figure 9. (a) An overview and (b) detailed HR-TEM image of graphene nanosheets synthesized from isopropanol precursor.

Table 1. Dependence of material properties and synthesis yield on process parameters. $P = 195$ W. $I_{D/G}$, $I_{2D/G}$—Raman band integrated intensity ratio, $I_{MAX\ D/G}$, $I_{MAX\ 2D/G}$—Raman band peak maximum ratio.

Q_{C2H2} (sccm)	Q_{H2} (sccm)	$I_{D/G}$	$I_{MAX\ D/G}$	$I_{2D/G}$	$I_{MAX\ 2D/G}$	2D FWHM (cm^{-1})	XPS C1s sp^2/sp^3 ratio	Y_{FLG} (%)
6.5	—	1.6	1.2	0.4	0.1	147	5.6	37
6.5	6.5	0.6	0.5	1.3	0.7	53	9.5	42
6.5	13	0.5	0.4	1.5	0.8	50	16	39
6.5	19.5	0.6	0.4	1.3	0.7	58	12.5	36
19	38	0.6	0.5	1.5	0.8	54	50	47

acetylene synthesized FLG. 1-propanol sample also exhibited small intensity D^* (1210 cm^{-1}) and D^{**} (1450 cm^{-1}) peaks, suggesting more defects in the nanosheet's structure than in the case of isopropanol samples.

XPS analysis of prepared samples (figure S6) showed a very low content of oxygen, below 1.5 at%, and no nitrogen was detected in the samples. The ratio of sp^2/sp^3 determined from fitting C1s peak profile was approximately the same for both precursors, 16 and 13 for 1-propanol and isopropanol, respectively.

TGA and DTG curves of 1-propanol and isopropanol synthesized nanopowders can be seen in figure 11. Both samples exhibited very similar behaviour with weight loss maximum at 760 °C. The 1-propanol sample showed slightly lower temperature stability at temperatures between 300 °C and 650 °C. As showed in our previous work [35], the defective structure of the FLG can be correlated with mass loss in this temperature region and this was in agreement with the slightly higher intensity of defect-related Raman bands (D^*, D and D^{**}) in the 1-propanol sample.

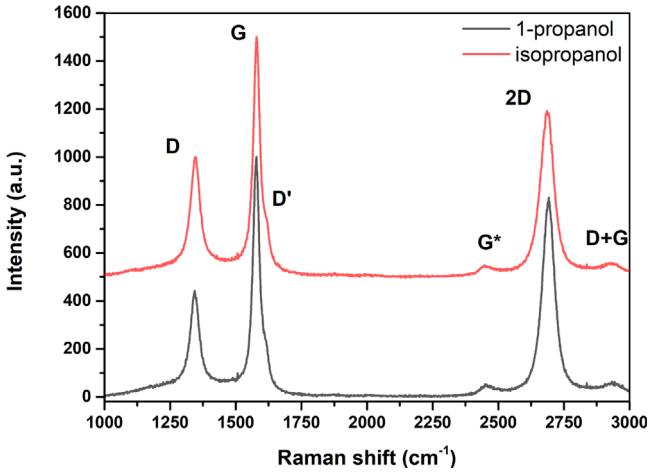

Figure 10. Raman spectroscopy of FLG graphene prepared from 1-propanol and isopropanol precursors, $Q_{1\text{-prop}} = 9$ sccm, $Q_{\text{isoprop}} = 19$ sccm, respectively. Argon flow rates $Q_c = 500$ sccm, $Q_s = 700$ sccm and $P = 160$ W.

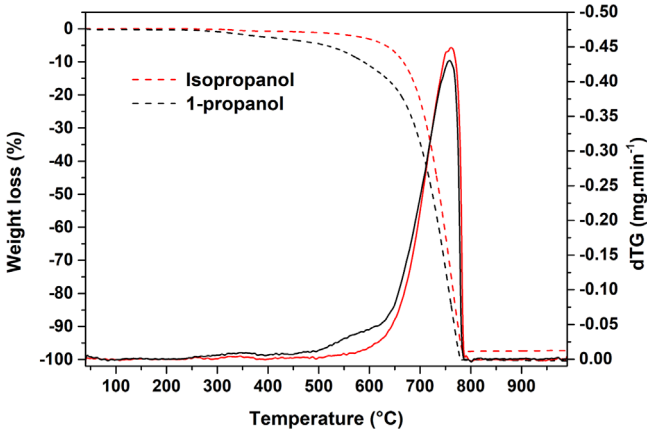

Figure 11. TG (dashed line—left axis) and DTG (solid line—right axis) analysis of FLG prepared from 1–propanol (black) and isopropanol (red) precursors, $Q_{1\text{-prop}} = 9$ sccm, $Q_{\text{isoprop}} = 19$ sccm, Argon flow rates $Q_c = 500$ sccm, $Q_s = 700$ sccm and $P = 160$ W.

The yield of synthesis was substantially lower than for acetylene, 14% and 8% but comparable with the synthesis from ethanol [16]. The yield of both these syntheses was naturally limited by a formation of highly stable CO molecules [10] and thus a lower amount of carbon available for the growth of FLG structure.

This result showed that the stable high-temperature environment formed by dual-channel microwave plasma torch discharge together with sufficient C:H ratio, 1:2 and higher in the precursor, led to their successful decomposition into basic organic precursors, such as C_2H_5, CH_3, and C_2H_2, followed by their dehydrogenation and formation of FLG nanosheets. The admixture of H_2, 10 sccm, to 1-propanol and isopropanol, had only a very small influence on the synthesis process. Due to the flow rate ratio 1:2 of 1-propanol to isopropanol and constant admixture of H_2, 10 sccm, we were able to investigate the influence of gas mixture with different C:H ratio. Even so, in both cases, we observed only a small decrease of yield, by 1%, and the material analysis by Raman spectroscopy and XPS (figures S6 and S7) showed only minor changes in comparison to material synthesized without hydrogen admixture. The yield decrease could be understood in terms of the reverse hydrogenation process of C_2H and C_2 molecules when more gas-phase hydrocarbons are formed (figure 1) and the amount of solid-state product decreases. This result is in agreement with the yield decrease of FLG and the analysis of decomposition products of ethanol formed in our microwave plasma torch discharge [33]. Together with previously reported FLG synthesis from ethanol (C_2H_5OH) and its isomer, dimethyl ether (CH_3OCH_3) by Dato *et al* [14], our results showed that the synthesis using alcohols with the same stoichiometry is independent of the precursor molecular arrangement. All the precursors are initially decomposed into hydrocarbon-related fragments such as CH_3, C_2H_5, or C_3H_7 and oxygen-related fragments containing predominantly carbon–oxygen groups such as OH, H_2COH, or HCOH. Groups containing oxygen are gradually converted into CO and H2 and do not contribute to graphene growth. Similarly, any collision of the OH group or free oxygen atom with hydrocarbon fragments leads to the formation of CO [11] and a loss of the carbon atom in the graphene growth process. Based on our result, this limit in the yield of alcohol-based precursor synthesis can be improved by using higher alcohols. Our synthesis using isopropanol had significantly increased the yield from 7% to 14% in comparison to ethanol [33].

It is also interesting to compare the yield of the synthesis from the point of view of the number of carbon atoms available for graphene growth. If we consider that in the case of 1-propanol and isopropanol one carbon atom is lost due to the formation of CO molecules, we have two carbon atoms available for FLG synthesis, the same as in the case of C_2H_2. Yet, the yield using C_2H_2 is three times higher than in the case of isopropanol, 47 versus 14% for the same flow rate of 19 sccm. This shows the importance of the arrangement of precursor molecules and subsequent reaction pathways during the decomposition process on the formation of C atoms and C_2 molecules. We can see this effect also in the case of isopropanol and 1-propanol precursors. Although both precursors generated material of the same quality, the synthesis yield using isopropanol was twice that of 1-propanol. In our opinion, the main reason for the different yield is again the molecular arrangement of the precursor. The pyrolysis of 1-propanol [36] generates longer hydrocarbon chains than isopropanol [37] resulting in the variation of reaction pathway and consequently lower yield.

4. Conclusions

The admixture of hydrogen provided a crucial step in the high-efficiency synthesis, 47%, of high-quality FLG nanosheets, D/G and 2D/G Raman peak ratio of 0.5 and 1.5, respectively, from acetylene. The transition from highly defective solid carbon to good quality FLG material provides important evidence of the role of the dehydrogenation process in the graphene gas phase growth mechanism hypothesis. A high-temperature environment formed by atmospheric pressure microwave plasma together with hydrogen generated by decomposition of higher alcohols, 1-propanol, and isopropanol, led to the successful synthesis of

FLG, but at a lower yield, 7 and 14%, respectively. Alcohol precursor with carbon to hydrogen ratio of 3:8 was sufficient to sustain dehydrogenation reaction during the gas phase growth even when the presence of the oxygen led to the formation of the highly stable CO molecule and lowered the yield of the synthesis. While the atom arrangement in the precursor molecule did not influence the synthesized material properties, the yield of the synthesis process showed strong dependence on the initial decomposition reactions of the precursor.

In conclusion, the use of an atmospheric pressure microwave plasma torch for the highly efficient synthesis of FLG from simple hydrocarbons represents a simple, fast, easily scalable, and environmentally friendly method to produce the graphene powder in large quantities comparable to liquid exfoliation methods.

Acknowledgments

This work was supported by The Czech Science Foundation under project 18-08520S and in part by project LM2018097 funded by the Ministry of Education, Youth and Sports of the Czech Republic. CzechNanoLab project LM2018110 funded by MEYS CR is gratefully acknowledged for the financial support of the HR-TEM and XPS measurements at CEITEC Nano Research Infrastructure.

Data availability statement

The data that support the findings of this study are available upon reasonable request from the authors.

Declaration of competing interest

The authors declare no conflicts of interests.

ORCID iDs

Ondřej Jašek https://orcid.org/0000-0002-1416-794X
Jozef Toman https://orcid.org/0000-0002-8391-8073
Miroslav Šnírer https://orcid.org/0000-0003-0534-5262
Jana Jurmanová https://orcid.org/0000-0001-8775-1680
Vít Kudrle https://orcid.org/0000-0002-7669-1691
Jan Michalička https://orcid.org/0000-0001-6231-0061
Dalibor Všianský https://orcid.org/0000-0001-9769-072X
David Pavliňák https://orcid.org/0000-0001-9669-7946

References

[1] Sun Y, Yang L, Xia K, Liu H, Han D, Zhang Y and Zhang J 2018 'Snowing' graphene using microwave ovens *Adv. Mater.* **30** 1803189
[2] Kim K S, Seo J H, Nam J S, Ju W T, Paek K H and Hong S H 2004 Production of hydrogen and carbon black by methane decomposition using DC-RF hybrid thermal plasmas *The 31st IEEE Int. Conf. on Plasma Science* ICOPS 2004. IEEE Conference Record—Abstracts
[3] Kim K S, Hong S H, Lee K-S and Ju W T 2007 Continuous synthesis of nanostructured sheetlike carbons by thermal plasma decomposition of methane *IEEE Trans. Plasma Sci.* **35** 434–43
[4] Amirov R, Shavelkina M, Alihanov N, Shkolnikov E, Tyuftyaev A and Vorob'eva N 2015 Direct synthesis of porous multilayer graphene materials using thermal plasma at low pressure *J. Nanomater.* **2015** 1–6
[5] Zhong R and Hong R 2020 Continuous preparation and formation mechanism of few-layer graphene by gliding arc plasma *Chem. Eng. J.* **387** 124102
[6] Sun Y, Chen Z, Gong H, Li X, Gao Z, Xu S, Han X, Han B, Meng X and Zhang J 2020 Continuous 'snowing' thermotherapeutic graphene *Adv. Mater.* **32** 2002024
[7] Wang C, Sun L, Dai X, Li D, Chen X, Xia W and Xia W 2019 Continuous synthesis of graphene nano-flakes by a magnetically rotating arc at atmospheric pressure *Carbon* **148** 394–402
[8] Shavelkina M B, Filimonova E A and Kh Amirov R 2020 Effect of helium/propane–butane atmosphere on the synthesis of graphene in plasma jet system *Plasma Sources Sci. Technol.* **29** 025024
[9] Dato A, Radmilovic V, Lee Z, Phillips J and Frenklach M 2008 Substrate-free gas-phase synthesis of graphene sheets *Nano Lett.* **8** 2012–6
[10] Tatarova E, Dias A, Henriques J, do Rego A M B, Ferraria A M, Abrashev M V, Luhrs C C, Phillips J, Dias F M and Ferreira C M 2014 Microwave plasmas applied for the synthesis of free standing graphene sheets *J. Phys. D: Appl. Phys.* **47** 385501
[11] Tsyganov D *et al* 2016 On the plasma-based growth of 'flowing' graphene sheets at atmospheric pressure conditions *Plasma Sources Sci. Technol.* **25** 015013
[12] Melero C, Rincón R, Muñoz J, Zhang G, Sun S, Perez A, Royuela O, González-Gago C and Calzada M D 2018 Scalable graphene production from ethanol decomposition by microwave argon plasma torch *Plasma Phys. Control. Fusion* **60** 014009
[13] Fronczak M, Fazekas P, Károly Z, Hamankiewicz B and Bystrzejewski M 2017 Continuous and catalyst free synthesis of graphene sheets in thermal plasma jet *Chem. Eng. J.* **322** 385–96
[14] Dato A and Frenklach M 2010 Substrate-free microwave synthesis of graphene: experimental conditions and hydrocarbon precursors *New J. Phys.* **12** 125013
[15] Nepal A, Singh G P, Flanders B N and Sorensen C M 2013 One-step synthesis of graphene via catalyst-free gas-phase hydrocarbon detonation *Nanotechnology* **24** 245602
[16] Toman J, Jasek O, Snirer M, Kudrle V and Jurmanova J 2019 On the interplay between plasma discharge instability and formation of free-standing graphene nanosheets in a dual-channel microwave plasma torch at atmospheric pressure *J. Phys. D: Appl. Phys.* **52** 265205
[17] Jašek O, Toman J, Jurmanová J, Šnírer M, Kudrle V and Buršíková V 2020 Study of graphene layer growth on dielectric substrate in microwave plasma torch at atmospheric pressure *Diam. Relat. Mater.* **105** 107798
[18] Voráč J, Synek P, Potočňáková L, Hnilica J and Kudrle V 2017 Batch processing of overlapping molecular spectra as a tool for spatio-temporal diagnostics of power modulated microwave plasma jet *Plasma Sources Sci. Technol.* **26** 025010
[19] Carbone E, D'Isa F, Hecimovic A and Fantz U 2020 Analysis of the C2 ($d^3\Pi_g$–$a^3\Pi_u$) Swan bands as a thermometric probe in CO_2 microwave plasmas *Plasma Sources Sci. Technol.* **29** 055003
[20] Rincón R, Marinas A, Muñoz J, Melero C and Calzada M D 2016 Experimental research on ethanol-chemistry

decomposition routes in a microwave plasma torch for hydrogen production *Chem. Eng. J.* **284** 1117–26
[21] Harris S J and Weiner A M 1985 Chemical kinetics of soot particle growth *Annu. Rev. Phys. Chem.* **36** 31–52
[22] Frenklach M and Wang H 1991 Detailed modeling of soot particle nucleation and growth *Symp. (International) on Combustion* 23, 1559–66
[23] Marinov N M 1999 A detailed chemical kinetic model for high temperature ethanol oxidation *Int. J. Chem. Kinet.* **31** 183–220
[24] Zádor J, Fellows M D and Miller J A 2017 Initiation reactions in acetylene pyrolysis *J. Phys. Chem.* A **121** 4203–17
[25] Benson S W 1989 The mechanism of the reversible reaction: 2C2H2? Vinyl acetylene and the pyrolysis of butadiene *Int. J. Chem. Kinet.* **21** 233–43
[26] Back M H 1971 Mechanism of the pyrolysis of acetylene *Can. J. Chem.* **49** 2199–204
[27] Snirer M, Kudrle V, Toman J, Jašek O and Jurmanova J 2021 Structure of microwave plasma torch discharge during graphene synthesis from ethanol *Plasma Sources Sci. Technol.* **30** 065020
[28] Choi M, Altman I S, Kim Y-J, Pikhitsa P V, Lee S, Park G-S, Jeong T and Yoo J-B 2004 Formation of shell-shaped carbon nanoparticles above a critical laser power in irradiated acetylene *Adv. Mater.* **16** 1721–5
[29] Yang G, Li L, Lee W B and Ng M C 2018 Structure of graphene and its disorders: a review *Sci. Technol. Adv. Mater.* **19** 613–48
[30] Meunier J-L, Mendoza-Gonzalez N-Y, Pristavita R, Binny D and Berk D 2014 Two-dimensional geometry control of graphene nanoflakes produced by thermal plasma for catalyst applications *Plasma Chem. Plasma Process.* **34** 505–21
[31] Choi J-H, Li Z, Cui P, Fan X, Zhang H, Zeng C and Zhang Z 2013 Drastic reduction in the growth temperature of graphene on copper via enhanced London dispersion force *Sci. Rep.* **3** 1925
[32] Dato A 2019 Graphene synthesized in atmospheric plasmas—a review *J. Mater. Res.* **34** 214–30
[33] Toman J, Jašek O, Šnírer M, Pavliňák D, Navrátil Z, Jurmanová J, Chudják S, Krčma F, Kudrle V and Michalička J 2021 On the transition of reaction pathway during microwave plasma gas-phase synthesis of graphene nanosheets: from amorphous to highly crystalline structure *Plasma Process. Polym.* **18** e2100008
[34] Ferrari A C *et al* 2006 Raman spectrum of graphene and graphene layers *Phys. Rev. Lett.* **97** 187401
[35] Jašek O, Toman J, Všianský D, Jurmanová J, Šnírer M, Hemzal D, Bannov A G, Hajzler J, St'ahel P and Kudrle V 2021 Controlled high temperature stability of microwave plasma synthesized graphene nanosheets *J. Phys. D: Appl. Phys.* **54** 165201
[36] Barnard J A and Hughes H W D 1960 The pyrolysis of n-propanol *Trans. Faraday Soc.* **56** 64
[37] Barnard J A 1960 The pyrolysis of isopropanol *Trans. Faraday Soc.* **56** 72